Supplementary Materials

Pulsed Electrodeposition of Well-Ordered Nanoporous Cu-Doped Ni Arrays Promote High-Efficiency Overall Hydrazine Splitting

Qiangqiang Sun,[†a,*] Yibing Li,[†c] Jianfang Wang,[a] Baoyue Cao,[a] Yan Yu,[a] Chunsheng Zhou,[a] Guochun Zhang,[a] Zenglin Wang,[b,*] Chuan Zhao [c,*]

[a] Shaanxi Key Laboratory of Comprehensive Utilization of Tailings Resources, Research Centre of Grapheme Technology and Application, Shangluo University, Shangluo, 726000, China

[b] Key Laboratory of Applied Surface and Colloid Chemistry, Ministry of Education, and School of Chemistry and Chemical Engineering, Shaanxi Normal University, Xi'an, 710119, China

[c] School of Chemistry, The University of New South Wales, Sydney, NSW 2052, Australia

†These authors contribute equally to this work.

E-mail: sqq3c118@slxy.edu.cn; wangzl@snnu.edu.cn; chuan.zhao@unsw.edu.au

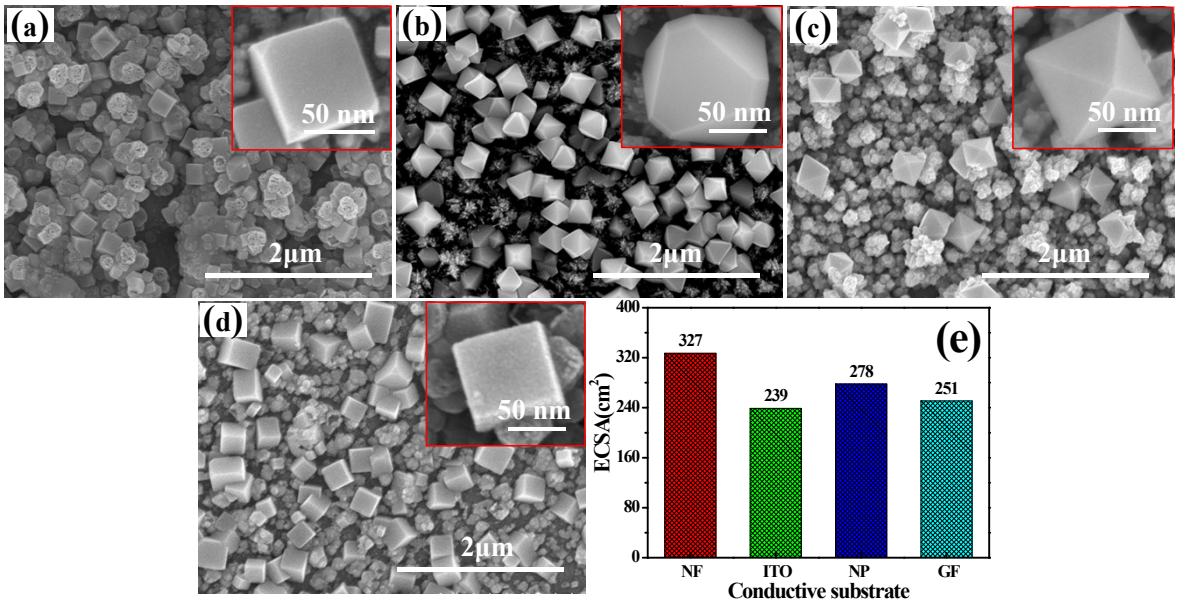

Fig. S1 (a-d) SEM images of NiCu NCs grown on different substrates and (e) the corresponding ECSAs during HER.

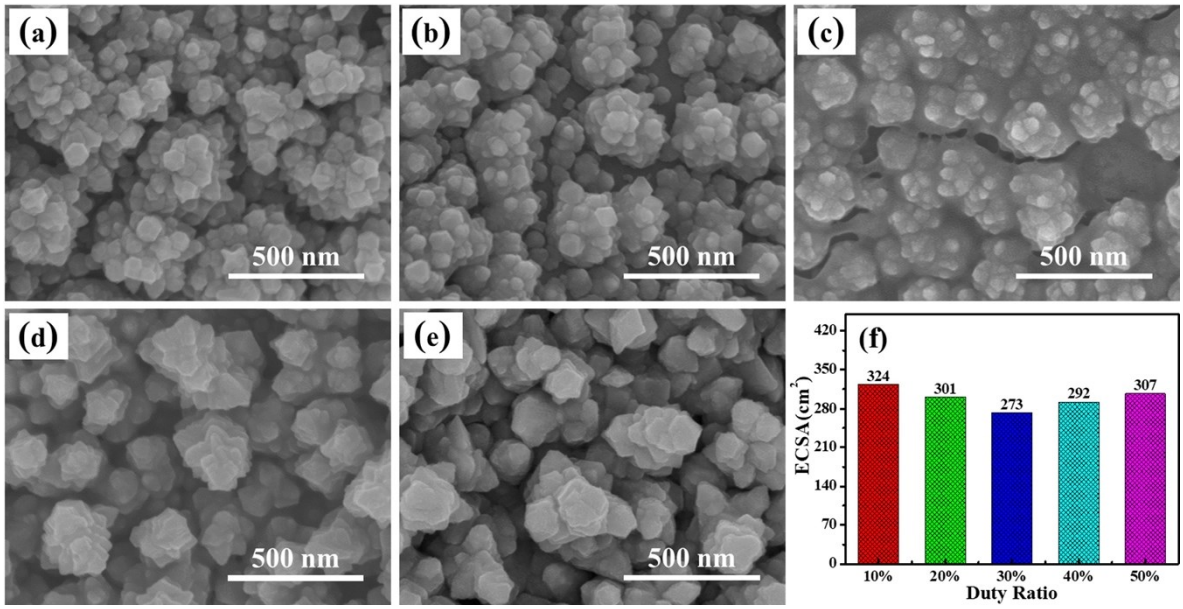

Fig. S2 (a-e) SEM images of NiCu NCs for various duty ratios and (f) the corresponding ECSAs during HER.

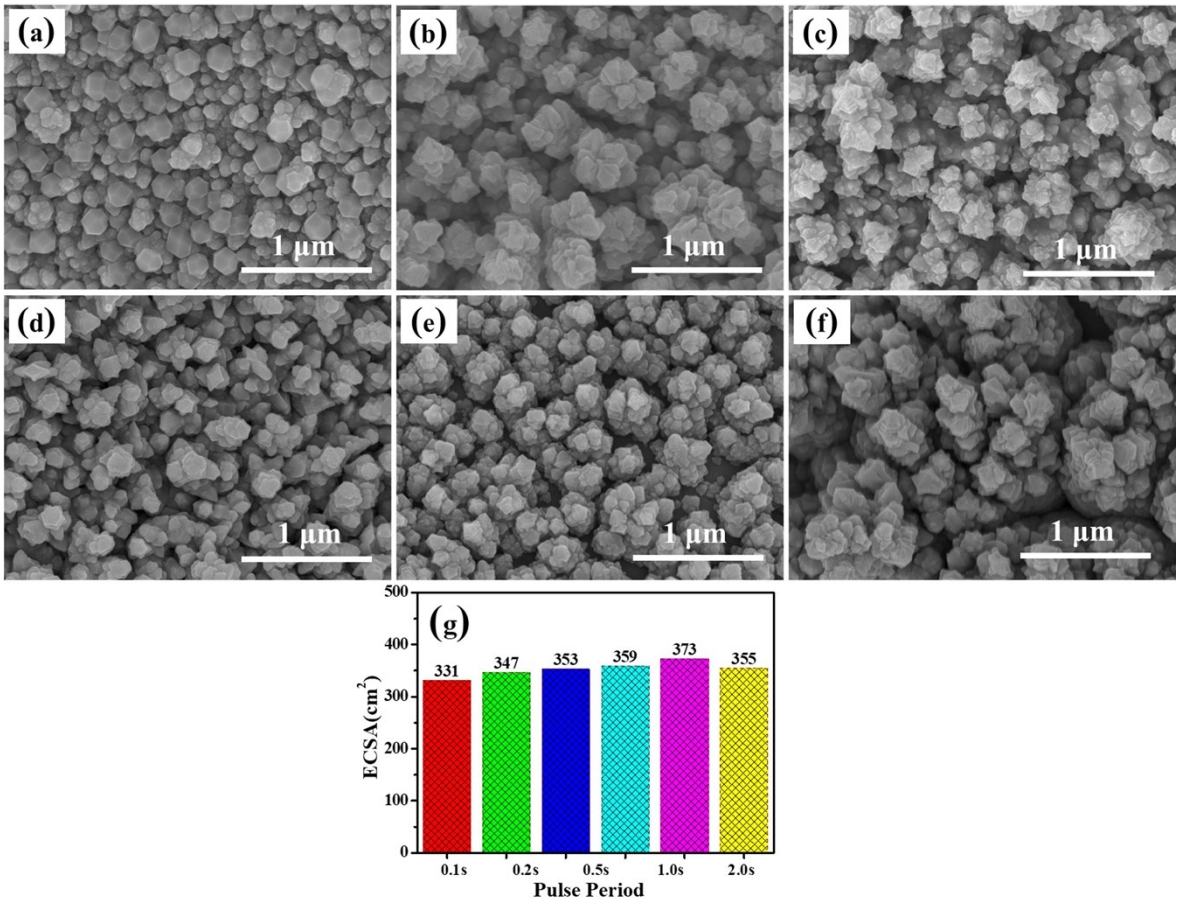

Fig. S3 (a-f) SEM images of NiCu NCs for different pulse periods and (g) the corresponding ECSAs during HER.

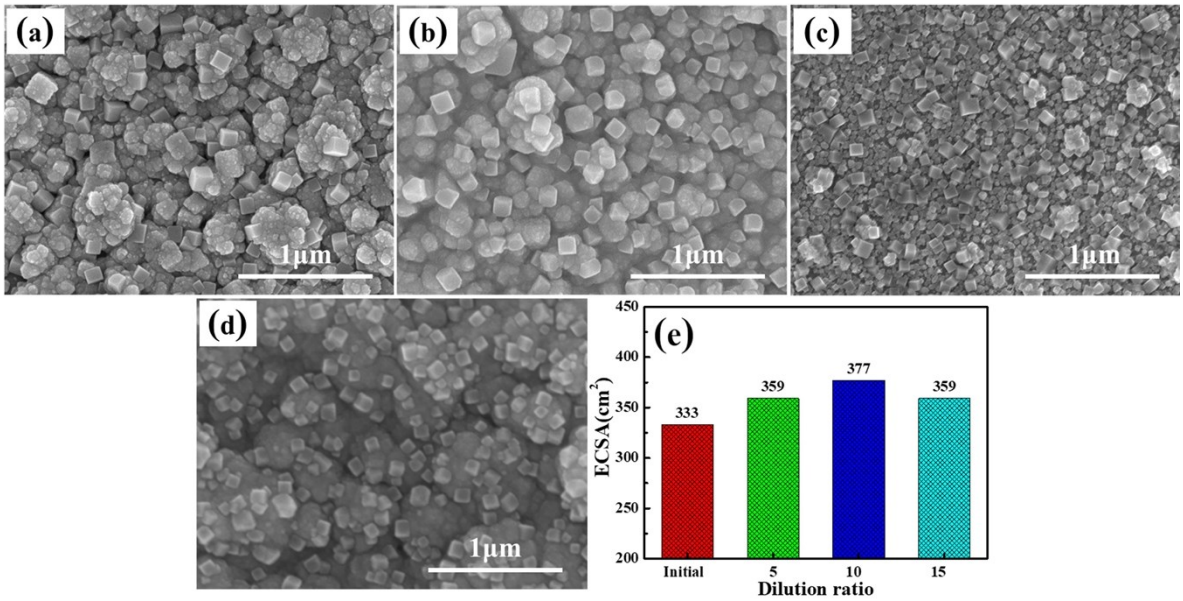

Fig. S4 (a-d) SEM images of NiCu NCs for different dilution ratios of initial electrolyte (containing 0.50 M $NiSO_4$, 0.075 M $CuSO_4$ and 0.50 M H_3BO_3 with pH of 4.0) and (e) the corresponding ECSAs during HER.

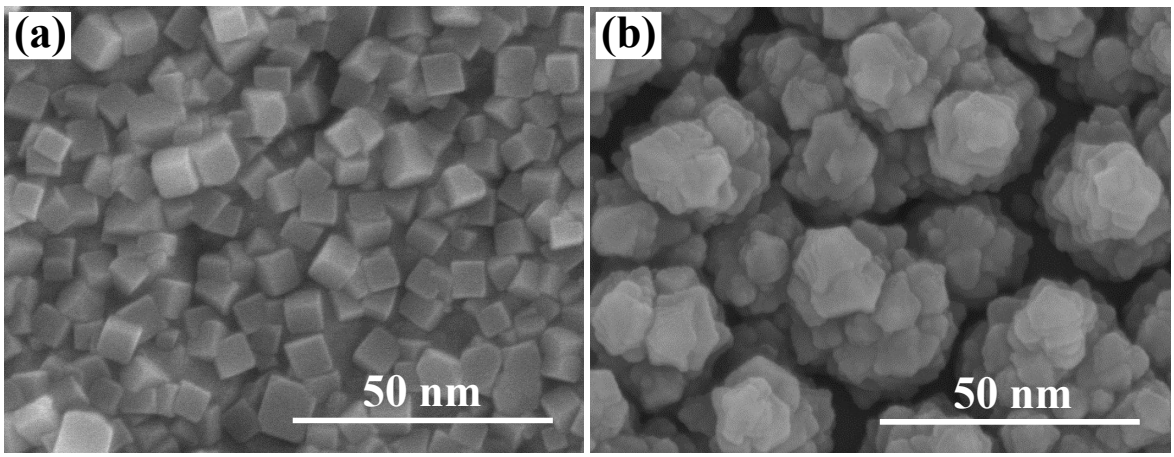

Fig. S5 SEM images of NiCu NCs for the contrast test with (a) presence and (b) absence of boric acid.

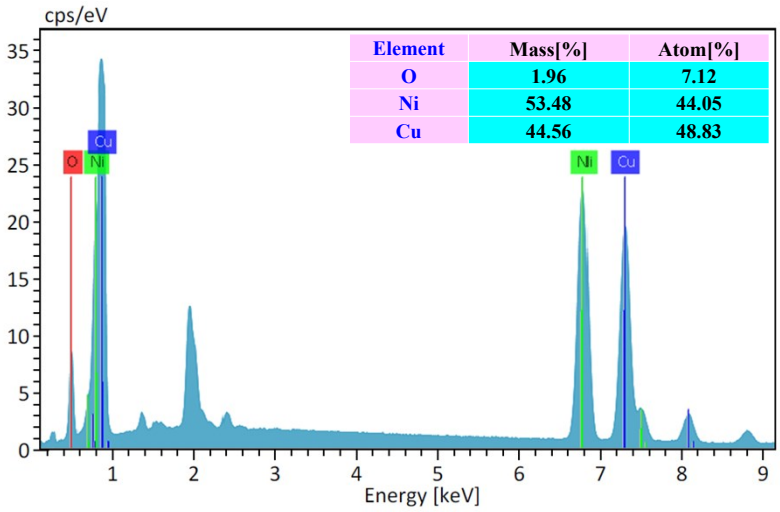

Fig. S6 EDX spectrum of NiCu nanocubes.

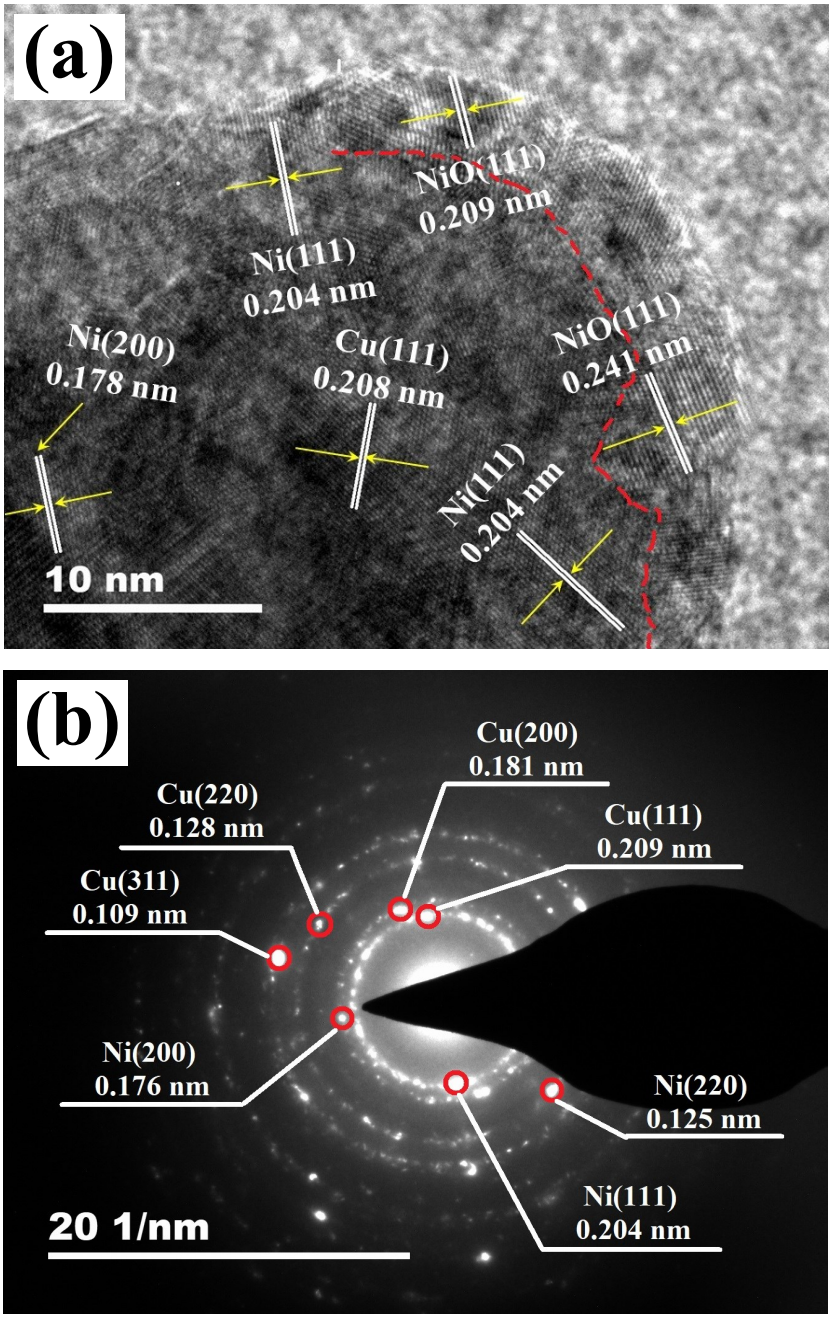

Fig.S7 (a) HRTEM image and (b) SAED pattern of NiCu NCs.

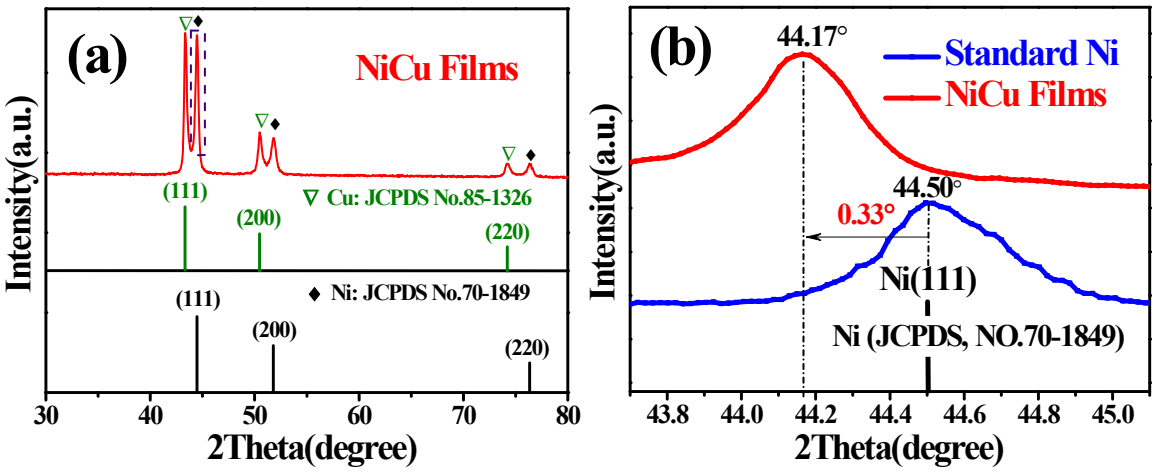

Fig. S8 (a)XRD patterns of NiCu NCs, (b) Comparison of diffraction peaks of Ni(111) for NiCu NCs with that of standard Ni Powder.

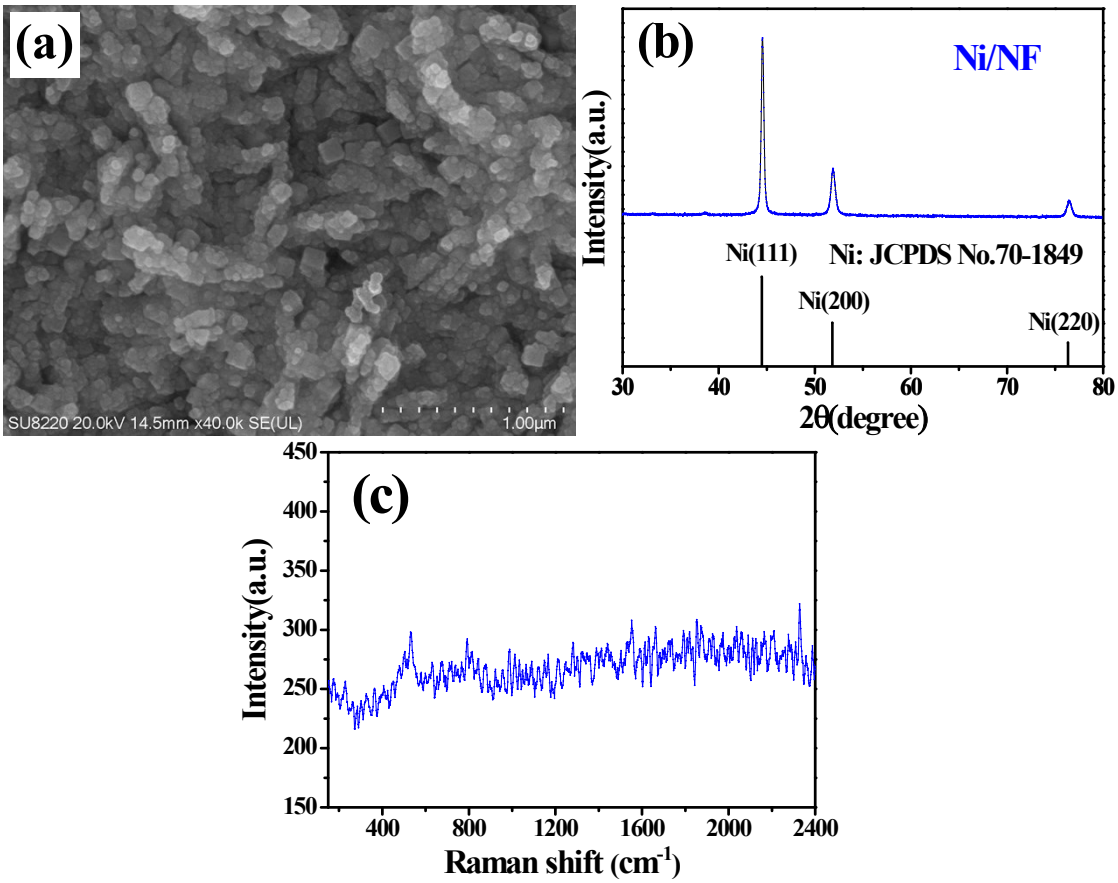

Fig. S9 (a)SEM image, (b) XRD pattern and (c) Raman spectrum of Ni/NF.

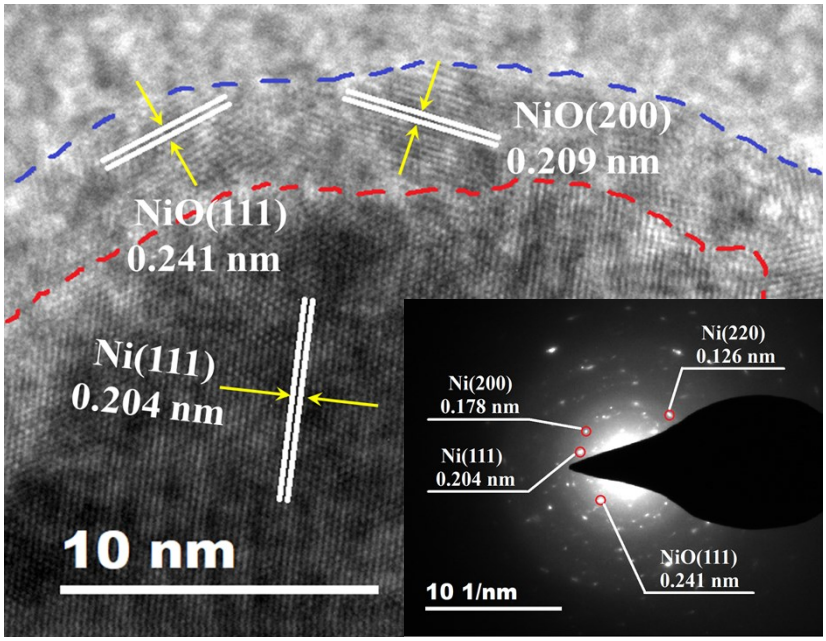

Fig.S10 HRTEM image of NiCu CNPs, insert: SAED pattern.

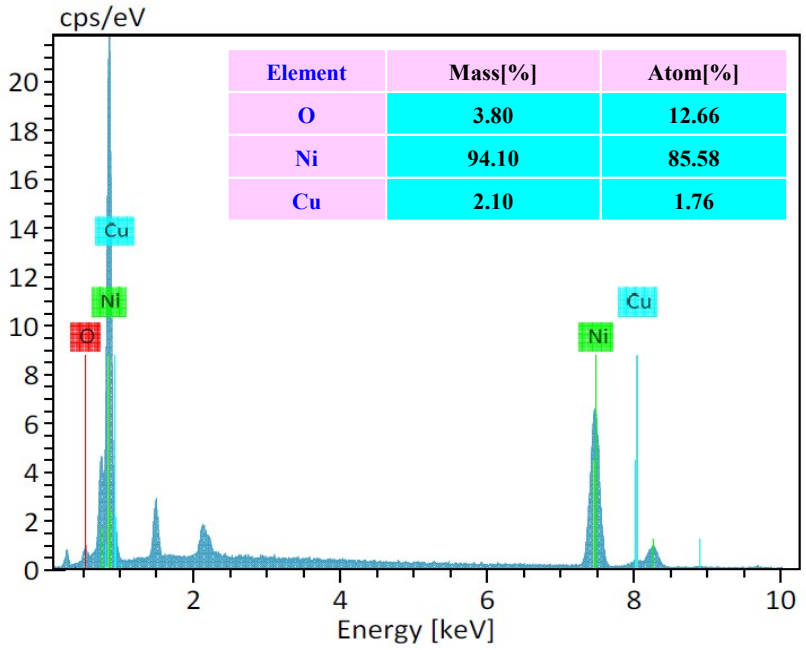

Fig. S11 EDX spectrum of Ni(Cu) cubic nanopores.

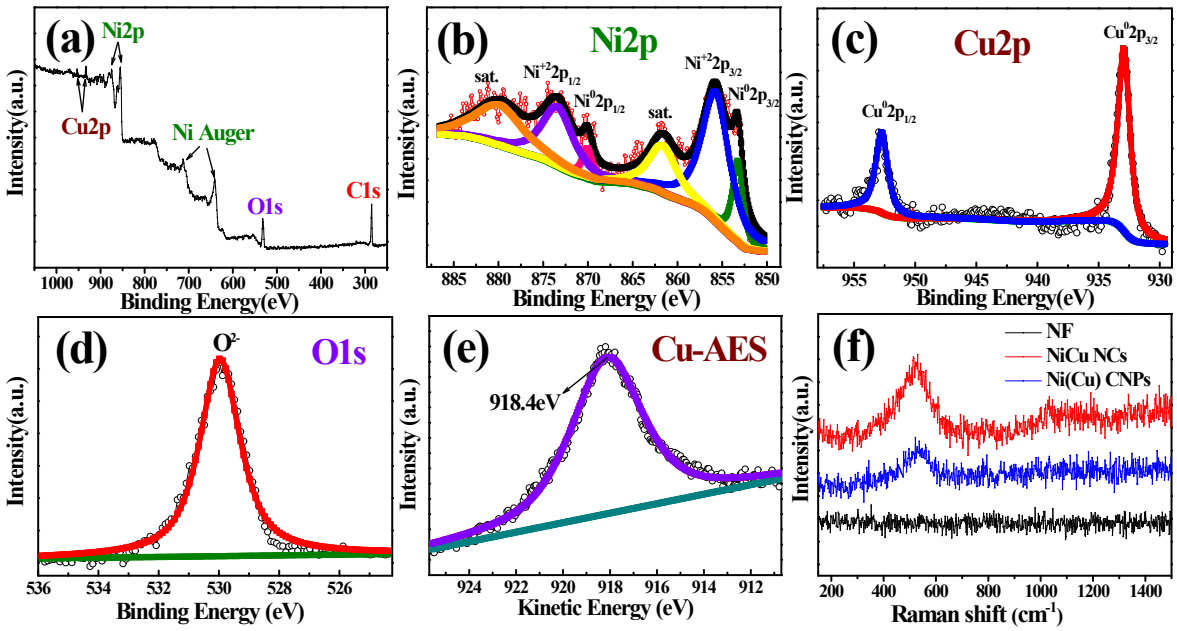

Fig. S12 (a) XPS survey and high-resolution XPS spectra of Ni(Cu) CNPs in (b)Ni 2p, (c)Cu 2p, (d)O 1s region, (e) Cu AES spectrum and (f) Raman spectra of Ni(Cu) CNPs.

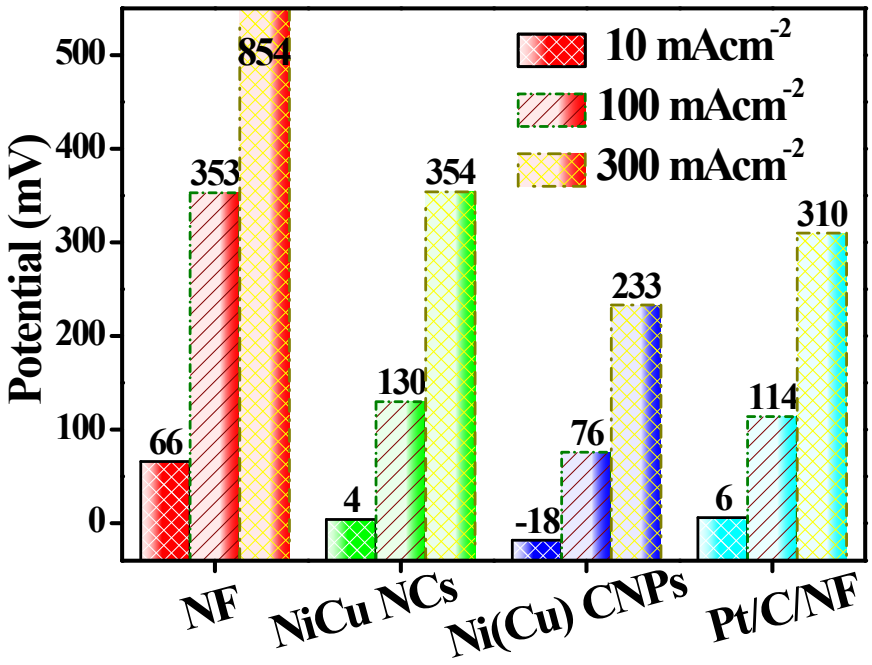

Fig. S13 Comparison of the working potentials for NF, NiCu NCs, Pt/C/NF and Ni(Cu) CNPs electrocatalysts toward HzOR at the anodic current densities of 10, 100, 300 $mAcm^{-2}$.

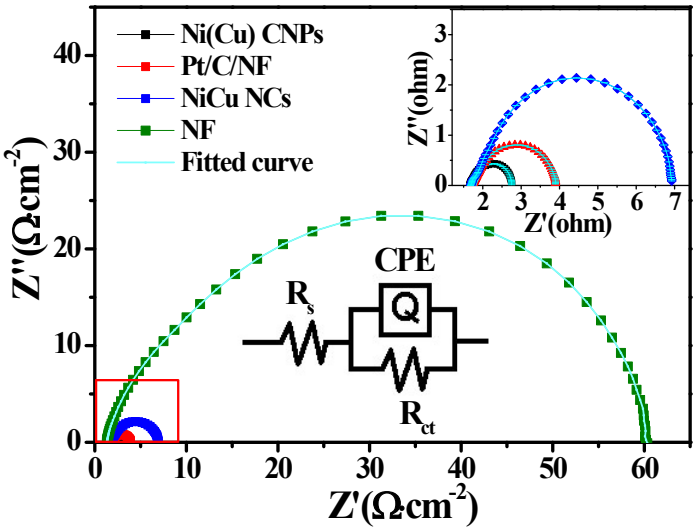

Fig. S14 Nyquist plots of NF, NiCu NCs, Pt/C/NF and Ni(Cu) CNPs electrodes towards HzOR.

Fig. S15 Optical image of the generated H_2 and N_2 gas bubble on the cathode and anode in the cell, respectively.

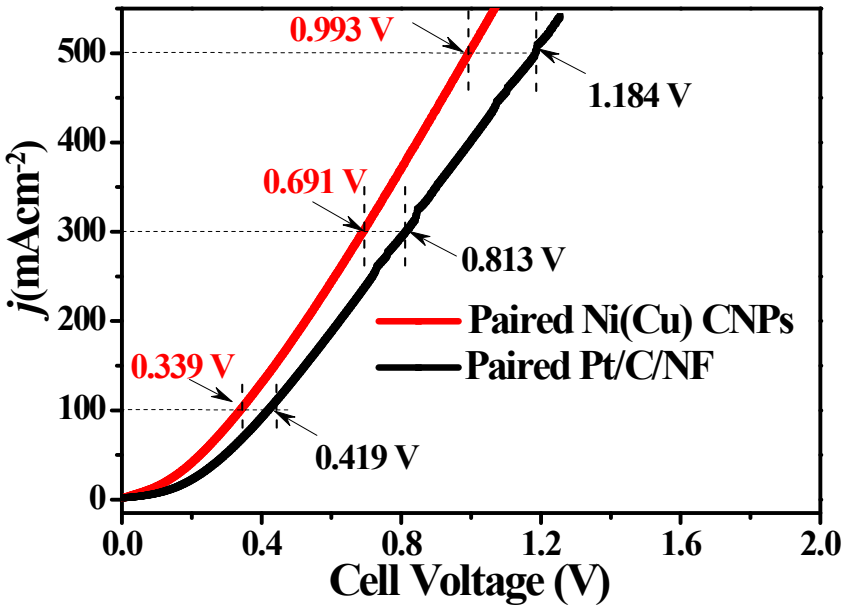

Fig. S16 The comparing LSV curves of Ni(Cu) CNPs || Ni(Cu) CNPs and Pt/C||Pt/C couples with a scan rate of 5 mVs^{-1} in the OHzS cell.

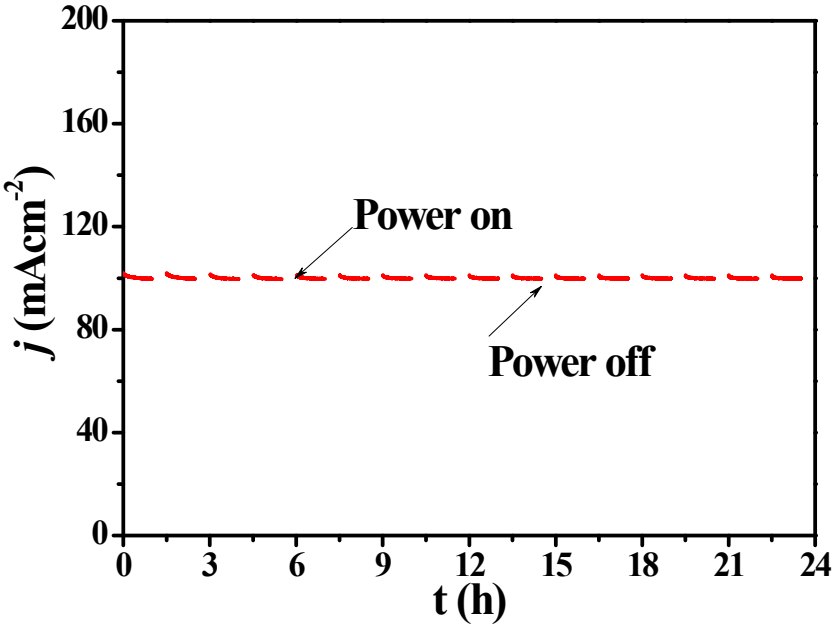

Fig. S17 Intermittent chronoamperograms of the Ni(Cu) CNPs/NF couple in the two-electrode cell at working potential of 0.340 V for 24 h with the periods of 1 h for continuous electrolysis and 0.5 h for power shutdowns.

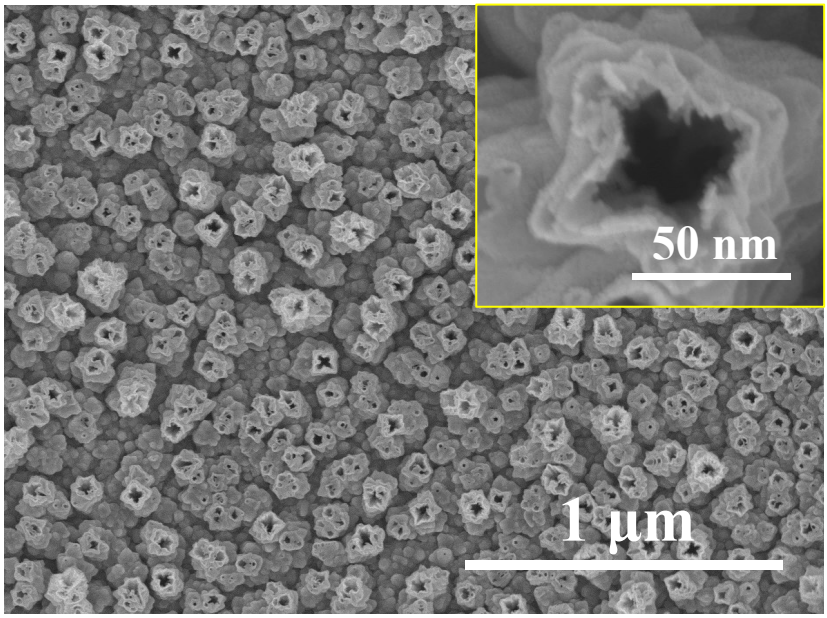

Fig. S18 SEM images of Ni(Cu) CNPs after 24 h continuous electrolysis in OHzS system.

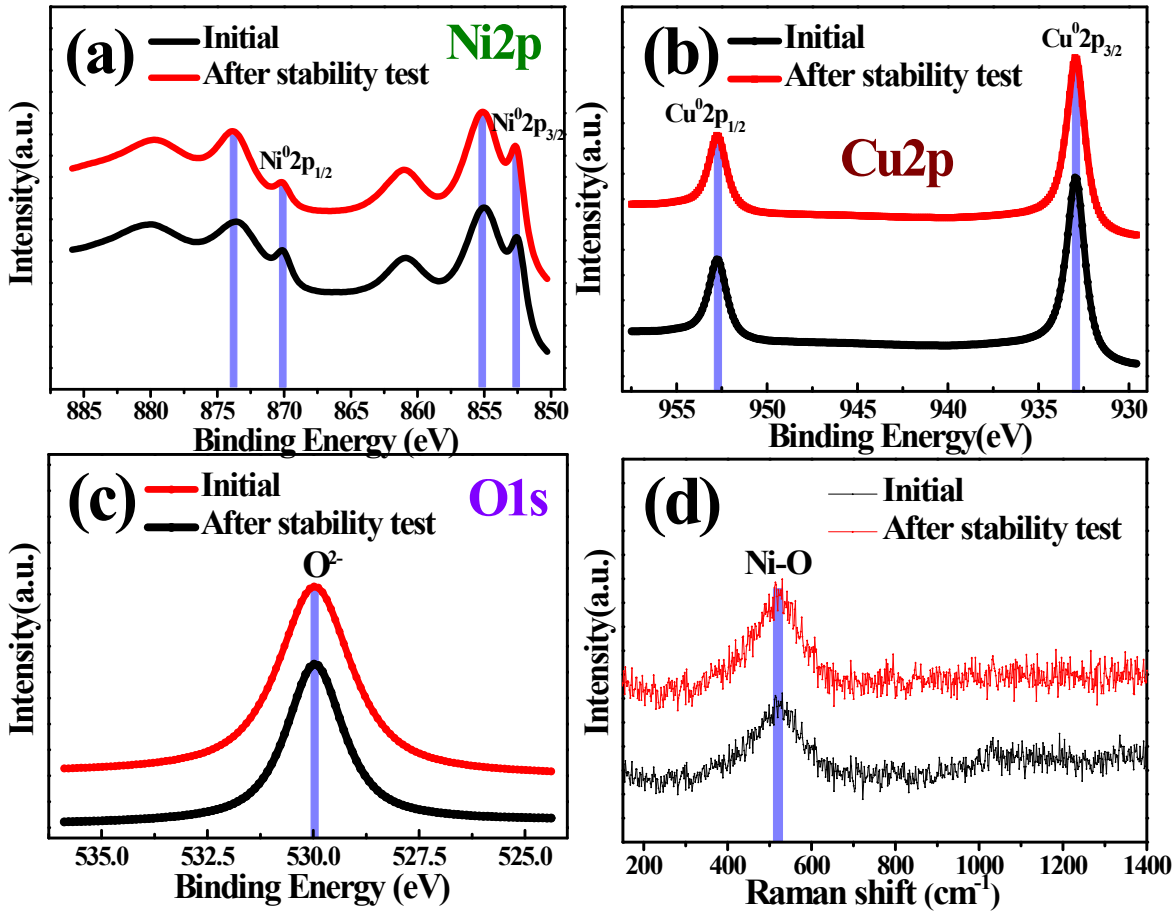

Fig. S19 (a-c) The compared high-resolution spectra of Ni 2p, Cu 2p and O 1s, and (d)the compared Raman spectra of Ni(Cu) CNPs before and after 24 h continuous electrolysis in OHzS system.

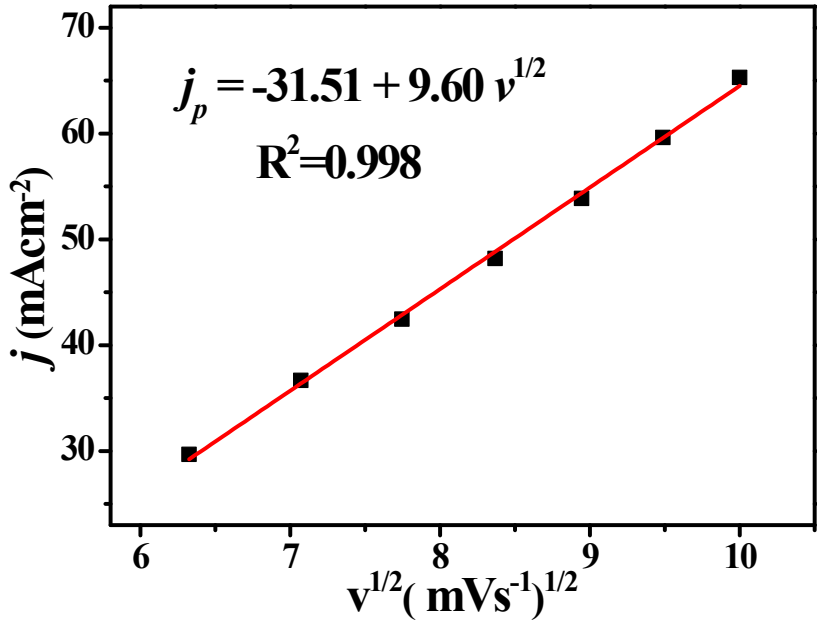

Fig. S20 Plot for the hydrazine oxidation current (j_p) versus the square root of scan rate ($v^{1/2}$).

Table S1. Comparison of HER activities of Ni(Cu) CNPs with other reported electrocatalysts in alkaline solutions.

Material	Electrolyte	Tafel slope/ $mVdec^{-1}$	η at j= 10 mA cm^{-2}	Ref
Ni(Cu) CNPs	**1 M KOH**	**51.1**	**41**	**This work**
NiMoN/NF	1 M KOH	45.6	56	S1
FeCoNi-HNTAs	1 M KOH	37.5	58	S2
Ni_3N/C	1 M KOH	48	64	S3
NiFeP@TiN/CC	1 M KOH	73.0	75	S4
NiFeP@/C	1 M KOH	92.6	79	S5
$NiFeO_x$/CFP	1 M KOH	84.6	88	S6
NiCoN/C	1 M KOH	-	103	S7
NiFeV/NF	1 M KOH	62.0	125	S8
Ni-Cu-3/Cu	1 M KOH	57.2	128	S9
Ni_5P_4/Ni foil	1 M KOH	53	150	S10
$Ni_{0.9}Fe_{0.1}$/NC-NF	1 M KOH	111	231	S11

Table S2. The EIS fit values of as-obtained electrodes during HER

Parameter \ Electrode	Ni(Cu) CNPs	NiCu NCs	Ni/NF	NF
$R_s/(\Omega \cdot cm^{-2})$	1.596	1.601	1.711	1.737
$R_{ct}/(\Omega \cdot cm^{-2})$	4.48	6.33	11.14	68.22

Table S3. Comparison of HzOR performances of Ni(Cu) CNPs with other recently reported electrocatalysts in alkaline solutions.

Material	Electrolyte	Current density ($mAcm^{-2}$)	Potential (mV)	Ref
Ni(Cu) CNPs	**0.5 M N_2H_4 +1 M KOH**	**10** **100** **300**	**-18** **76** **233**	**This work**
Co_3Ta/C	0.5 M N_2H_4 +3 M KOH	25.2	60	S12
$CuNi_2$-N	0.5 M N_2H_4 +1 M KOH	10	0.5	S13
Ni(Cu)/NF	0.5 M N_2H_4 +1 M KOH	100	108	S14
CoS_2/TiM	0.1 M N_2H_4+ 1 M KOH	100	125	S15
Fe-CoS_2	0.1 M N_2H_4 +1 M KOH	100	129	S16
$CoSe_2$/NF	0.5 M N_2H_4 +1 M KOH	100	170	S17
Ni_3S_2/NF	0.2 M N_2H_4 +1 M KOH	100	415	S18
$Ni_{0.43}Cu_{0.57}$/Cu	0.1 M N_2H_4 +3 M KOH	300	468	S19
NiCo	0.1 M N_2H_4 +1 M KOH	36	100	S20
$Ni_{0.6}Co_{0.4}$	0.5 M N_2H_4 +3 M KOH	292	218	S21

Table S4. The EIS fit values of as-obtained electrodes during HzOR

Parameter \ Electrode	Ni(Cu) CNPs	Pt/C/NF	NiCu NCs	NF
$R_s/(\Omega \cdot cm^{-2})$	1.787	1.792	1.799	1.696
$R_{ct}/(\Omega \cdot cm^{-2})$	1.12	2.08	5.32	54.93

Table S5. Comparison of Cell voltages for the OHzS system integrated by the previous reported bifunctional catalysts in alkaline solutions.

Two-electrode electrolyzer	Electrolyte	Cell voltage	Ref
Ni(Cu) CNPs‖Ni(Cu) CNPs	**1 M KOH +0.5 M N_2H_4**	**0.070 V for 10 mA cm^{-2} 0.339 V for 100 mA cm^{-2} 0.527 V for 200 mA cm^{-2} 0.691 V for 300 mA cm^{-2}**	**This work**
$CoSe_2$/NF‖$CoSe_2$/NF	1 M KOH +0.5 M N_2H_4	0.164 V for 10 mA cm^{-2}	S17
Cu_1Ni_2-N‖Cu_1Ni_2-N	1 M KOH +0.5 M N_2H_4	0.240 V for 10 mA cm^{-2}	S13
Ni(Cu)/NF‖Ni(Cu)/NF	1 M KOH +0.5 M N_2H_4	0.41 V for 100 mA cm^{-2}	S14
Ni_2P/NF‖Ni_2P/NF	1 M KOH +0.5 M N_2H_4	0.45 V for 100 mA cm^{-2}	S22
Fe-CoS_2‖Fe-CoS_2	1 M KOH +0.1 M N_2H_4	0.610 V for 100 mA cm^{-2}	S16
Cu_3P/CF‖Cu_3P/CF	1 M KOH +0.5 M N_2H_4	0.720 V for 100 mA cm^{-2}	S23
NiS_2/TiM‖NiS_2/TiM	1 M KOH +0.5 M N_2H_4	0.750 V for 100 mA cm^{-2}	S24
CoS_2/TiM‖CoS_2/TiM	1 M KOH +0.1 M N_2H_4	0.810 V for 100 mA cm^{-2}	S15

References

[1] L. Yu, Q. Zhu, S. W. Song, B. McElhenny, D. Z. Wang, C. Z. Wu, Z. J. Qin, J. M. Bao, Y. Yu, S. Chen, Z. F. Ren, Non-noble metal-nitride based electrocatalysts for high-performance alkaline seawater electrolysis. *Nat. Commun.*, 2019, **10**, 5106.

[2] H. Y. Li, S. M. Chen, Y. Zhang, Q. H. Zhang, X. F. Jia, Q. Zhang, L. Gu, X. M. Sun, L. Song, X. Wang, Systematic design of superaerophobic nanotubearray electrode comprised of transition-metal sulfides for overall water splitting. *Nat. Commun.*, 2018, **9**, 2452.

[3] W. Ni, A. Krammer, C. S. Hsu, H. M. Chen, A. Schüler, X. Hu, Ni_3N as an active hydrogen oxidation reaction catalyst in alkaline medium. *Angew. Chem. Int. Ed.*, 2019, **58**, 1-6.

[4] X. Peng, A. M. Qasim, W. H. Jin, L. Wang, L. S. Hu, Y. P. Miao, W. Li, Y. Li, Z. T. Liu, K. F. Huo, K.Y. Wong, P. K. Chu, Ni-Doped Amorphous Iron Phosphide Nanoparticles on TiN Nanowire Arrays: An Advanced Alkaline Hydrogen Evolution Electrocatalyst, *Nano Energy*, 2018, **53**, 66-73.

[5] S. H. Ahn, A. Manthiram, Direct growth of ternary Ni-Fe-P porous nanorods onto nickel foam as a highly active, robust bifunctional electrocatalyst for overall water splitting, *J. Mater. Chem. A*, 2017, **5**, 2496-2503.

[6] H. T. Wang, H. W. Lee, Y. Deng, Z. Y. Lu, P. C. Hsu, Y. Y. Liu, D. C. Lin, Y. Cui, Bifunctional non-noble metal oxide nanoparticle electrocatalysts through lithium-induced conversion for overall water splitting. *Nat.Commun.*, 2015, **6**, 7261.

[7] J. Lai, B. Huang, Y. Chao, X. Chen, S. Guo, Strongly coupled nickel–cobalt nitrides/carbon hybrid nanocages with Pt-like activity for hydrogen evolution catalysis. *Adv. Mater.*, 2019, **31**, 1805541.

[8] K. N. Dinh, P. L. Zheng, Z. F. Dai, Y. Zhang, R. Dangol, Y. Zheng, B. Li, Y. Zong, Q. Y. Yan, Ultrathin Porous NiFeV Ternary Layer Hydroxide Nanosheets as a Highly Efficient Bifunctional Electrocatalyst for Overall Water Splitting, *Small*, 2018, **14**, 1703257.

[9] M. Y. Gao, C. Yang, Q. B. Zhang, Y. W. Yu, Y. X. Hua, Y. Li, P. Dong, Electrochemical fabrication of porous Ni-Cu alloy nanosheets with high catalytic activity for hydrogen evolution, *Electrochim. Acta*, 2016, **215**, 609-616.

[10] M. Ledendecker, S. K. Calderón, C. Papp, H. Steinrück, M. Antonietti, M. Shalom, The Synthesis of Nanostructured Ni_5P_4 Films and their Use as a Non-Noble Bifunctional Electrocatalyst for Full Water Splitting, *Angew. Chem. Int. Ed.*, 2015, **54**, 12361-12365.

[11] X. Zhang, H. Xu, X. Li, Y. Li, T. Yang, Y. Liang, Facile synthesis of nickel-iron/nanocarbon hybrids as advanced electrocatalysts for efficient water splitting. *ACS Catal.*, 2016, **6**, 580-588.

[12] G. Feng, L. An, B. Li, Y. X. Zuo, J. Song, F. H. Ning, N. Jiang, X. P. Cheng, Y. F. Zhang, D. G. Xia, Atomically ordered non-precious Co_3Ta intermetallic nanoparticles as high-performance catalysts for hydrazine electrooxidation. *Nat. Commun.,* 2019, **10**, 4514.

[13] Z. Y Wang, L. Xu, F. Z. Huang, L. B. Qu, J. T. Li, K. A. Owusu, Z. A. Liu, Z. F. Lin, B. H. Xiang, X. Liu, K. N. Zhao, X. B. Liao, W. Yang, Y. B. Cheng, L. Q. Mai, Copper–nickel nitride nanosheets as efficient bifunctional catalysts for hydrazine-assisted electrolytic hydrogen production. *Adv. Energy Mater.,* 2019, **9**, 1900390.

[14] Q. Q. Sun, L. Y. Wang, Y. Q. Shen, M. Zhou, Y. Ma, Z. L. Wang, C. Zhao, Bifunctional Copper-Doped Nickel Catalysts Enable Energy-Efficient Hydrogen Production via Hydrazine Oxidation and Hydrogen Evolution Reduction, *ACS Sustainable Chem. Eng.*, 2018, **6**, 12746-12754.

[15] X. Ma, J. M. Wang, D. N. Liu, R. M. Kong, S. A. Hao, G. Du, A. M. Asiri, X. P. Sun, Hydrazine-assisted electrolytic hydrogen production: CoS_2 nanoarray as a superior bifunctional electrocatalyst, *New J. Chem.*, 2017, **41**, 4754-4757.

[16] X. J. Liu, J. He, S. Z. Zhao, Y. P. Liu, Z. Zhao, J. Luo, G. Z. Hu, X. M. Sun, Y. Ding, Self-powered H_2 production with bifunctional hydrazine as sole consumable. *Nat. Commun.*, 2018, **9**, 4365.

[17] J.Y. Zhang, H. M. Wang, Y. F. Tian, Y. Yan, Q. Xue, T. He, H. F. Liu, C. D. Wang, Y. Chen, B. Y. Xia, Anodic Hydrazine Oxidation Assists Energy-Efficient Hydrogen Evolution over a Bifunctional Cobalt Perselenide Nanosheet Electrode, *Angew. Chem. Int. Ed.*, 2018, **57**, 7649-7653.

[18] G. Q. Liu, Z. T. Sun, X. Zhang, H. J. Wang, G. Z. Wang, X. J. Wu, H. M. Zhang, H. J. Zhao, Vapor-phase hydrothermal transformation of a nanosheet array structure $Ni(OH)_2$ into ultrathin Ni_3S_2 nanosheets on nickel foam for high-efficiency overall water splitting. *J. Mater. Chem. A*, 2018, **6**, 19201-19209.

[19] M. Sun, Z. Y. Lu, L. Luo, Z. Chang, X. M. Sun, A 3D porous Ni-Cu alloy film for high performance hydrazine electrooxidation. *Nanoscale*, 2016, **8**, 1479-1484.

[20] H. Wang, Y. J. Ma, R. F. Wang, J. L. Key, V. Linkov, S. Ji, Liquid-liquid interface-mediated room temperature synthesis of amorphous NiCo pompoms from ultrathin nanosheets with high catalytic activity for hydrazine oxidation. *Chem.Commun.*, 2015, **51**, 3570-3573.

[21] G. Feng, Y. Kuang, P. S. Li, N. N. Han, M. Sun, G. X. Zhang, X. M. Sun, Single crystalline ultrathin Nickel-Cobalt alloy nanosheets array for direct hydrazine fuel cells, *Adv. Sci.*, 2017, **4**, 1600179.

[22] C. Tang, R. Zhang, W. B. Lu, Z. Wang, D. N. Liu, S. Hao, G. Du, A. M. Asiri, X. P. Sun, Energy-saving electrolytic hydrogen generation: Ni_2P nanoarray as a high-performance non-noble-metal electrocatalyst, *Angew. Chem. Int. Ed.*, 2017, **56**, 842-846.

[23] M. Liu, R. Zhang, L. X. Zhang, D. N. Liu, S. A. Hao, G. Du, A. M. Asiri, R. M. Kong, X. P. Sun, Energy-efficient electrolytic hydrogen generation using a Cu_3P nanoarray as a bifunctional catalyst for hydrazine oxidation and water reduction, *Inorg. Chem. Front.*, 2017, **4**, 420-423.

[24] J. M. Wang, X. Ma, T. Y. Liu, L D. N. iu, S. A. Hao, G. Du, R. M. Kong, A. M. Asiri, X.P. Sun, NiS_2 nanosheet array: A high-active bifunctional electrocatalyst for hydrazine oxidation and water reduction toward energy-efficient hydrogen production, *Materials Today Energy,* 2017, **3**, 9-14.